Electronic Supplementary Material (ESI) for Physical Chemistry Chemical Physics.
This journal is © the Owner Societies 2017

Supplementary Information

Ionic Hydration-Induced Evolution of Decane-Water Interfacial Tension

Boyao Wen, [a] Chengzhen Sun, [a] Bofeng Bai, [a,] * Elizaveta Ya. Gatapova [b, c] and Oleg A. Kabov [b, c]

a. State Key Laboratory of Multiphase Flow in Power Engineering, Xi'an Jiaotong University, Xi'an, Shaanxi, 710049, China.

b. Kutateladze Institute of Thermophysics, Russian Academy of Sciences, Novosibirsk 630090, Russia

c. Novosibirsk State University, Novosibirsk 630090, Russia

* Corresponding Author. Tel: +86-029-82665316; Electronic mail: bfbai@mail.xjtu.edu.cn

Contents

1. Model and methods

1.1 Interaction potentials

1.1.1 OPLS All-Atom force field

In this paper, the OPLS All-Atom (OPLS-AA) force field[1] which can accurately describe the thermodynamic properties of organic liquids is employed to express the interactions between decane molecules. This force field is made up of four parts, *i.e.* non-bonded interactions, bond stretching, angle bending and torsion interactions:

$$E = E_{ab} + E_{bond} + E_{angle} + E(\phi) . \tag{S1}$$

The non-bonded interaction between a and b atom includes the standard 12/6 Lennard-Jones and Coulombic pairwise interactions, given by

$$E_{ab} = 4\varepsilon\left[\left(\frac{\sigma}{r_{ab}}\right)^{12} - \left(\frac{\sigma}{r_{ab}}\right)^{6}\right] + \frac{Cq_a q_b}{\chi r_{ab}} \qquad (r_{ab} < r_{cut}) , \tag{S2}$$

where ε is the depth of potential well, σ the distance at which the inter-atomic potential is zero, r_{cut} the cut-off radius, C an energy-conversion constant, q_a and q_b the charges of atom a and b, and χ is the dielectric constant. While r_{ab} is greater than r_{cut}, we use the Particle-Particle Particle-Mesh (PPPM) method to calculate the long-range electrostatic interactions. Potential parameters between the crossing atoms are obtained based on the Lorentz-Berthelot mixing rule,

$$\sigma_{ij} = \frac{\sigma_{ii} + \sigma_{jj}}{2} \qquad \varepsilon_{ij} = \sqrt{\varepsilon_{ii}\varepsilon_{jj}} \tag{S3}$$

All the LJ potential parameters are listed in **Table S1**.

Table S1. LJ potential parameters used in the simulations.

	ε (eV)	σ (Å)
O-O	6.611×10^{-3}	3.1507
H(H_2O)-H(H_2O)	1.999×10^{-3}	0.4000

C-C	2.864×10^{-3}	3.5000
H(Decane)-H(Decane)	1.302×10^{-3}	2.5000
O-H(H_2O)	3.364×10^{-3}	1.7753
O-C	4.351×10^{-3}	3.3254
O-H(Decane)	2.934×10^{-3}	2.8254
H(H_2O)-C	2.393×10^{-3}	1.9500
H(H_2O)-H(Decane)	1.613×10^{-3}	1.4500
C-H(Decane)	1.931×10^{-3}	3.0000
Na-Na	5.640×10^{-3}	2.3500
Na-O	6.106×10^{-3}	2.7504
Na-H(H_2O)	3.358×10^{-3}	1.3750
Na-C	4.019×10^{-3}	2.9250
Na-H(Decane)	2.710×10^{-3}	2.4250
Na-Cl	4.948×10^{-3}	3.3758
Cl-Cl	4.341×10^{-3}	4.4015
Cl -O	5.357×10^{-3}	3.7761
Cl-H(H_2O)	2.946×10^{-3}	2.4008
Cl-C	3.526×10^{-3}	3.9508
Cl-H(Decane)	2.377×10^{-3}	3.4508

The bond stretching and angle bending in the molecules are described by the *harmonic* potential as follows,

$$E_{bond} = K_{bond}(r_{ab} - r_0)^2, \tag{S4}$$

$$E_{angle} = K_{angle}(\theta - \theta_0)^2, \tag{S5}$$

where K_{bond} *and* K_{angle} are the bond and angle coefficients which are related to energy, r_0 is the equilibrium bond distance, and θ_0 is the equilibrium value of bond-angle.

The last term of the OPLS-AA potential is the torsion interaction, which are described by the *opls* dihedral style in our simulations. The form of *opls* dihedral style is as follows,

$$E(\phi) = \frac{V_1}{2}[1+\cos(\phi)] + \frac{V_2}{2}[1-\cos(2\phi)] + \frac{V_3}{2}[1+\cos(3\phi)], \quad \text{(S6)}$$

where V_1, V_2 and V_3 are the coefficients defined for dihedral. The detailed parameters of OPLS-AA potential can be found in **Reference S2**.[2]

1.1.2 TIP3P water model

In this study, we employ the TIP3P model to simulate the interactions between water molecules. The TIP3P water model is proven to be efficient and can precisely predict the structure and dynamics of the water phase. It assigns the charge and LJ parameter for each atom of the water molecule. Additionally, the *harmonic* bond and angle style are utilized to describe the O-H bond and the H-O-H angle. More detailed description and parameters can be found in **Reference S3**.[3]

1.2 Simulation details

In this paper, we adopt the Nose-Hoover method to keep the system balanced at specific temperature and pressure in the isothermal-isobaric (NPT) ensemble. The T_{damp} parameter determining the speed of the relaxation of temperature is a value of 0.2, while the P_{damp} determining the time scale on which pressure is relaxed is a value of 1. It is noteworthy that the good choice for the value of P_{damp} is about 1000 timesteps. In the case of lower value of P_{damp}, pressure and volume would fluctuate severely; in the case of higher value of P_{damp}, the equilibrium for pressure would be time-consuming. In order to reduce the storage requirements for data processing, the coordinates of ions and molecules are output every 25000 timesteps, *i.e.* 2.5 ps.

Because of the charge properties of ions, the long-range Coulombic interactions between ions or molecules play an important role in the simulation systems. Thus, in our simulations, we adopt the PPPM solver to calculate the long-range Coulombic force. In this method 3d FFTs is used to solve Poisson's equation on the mesh where atom charge is mapped, and then electric fields are interpolated on the mesh points back to the atoms. The PPPM solver is a more excellent method to reduce the computation time and memory storage, because it scales as Nlog(N) where N is the total atom numbers, which is far less than the

Ewald summation (N^(3/2)). The accuracy of PPPM method is 0.01 and the grid size of the mesh is 10 × 10 × 28 in the simulations.

1.3 Definition of interfacial thickness

As stated in the manuscript, we use the following hyperbolic tangent function to fit the density distribution curve of water and decane molecules.

$$\rho_i(z) = \frac{\rho_{i,bulk}}{2} - \frac{\rho_{i,bulk}}{2}\tanh\left(\frac{2(z-z_0)}{d}\right), \tag{S7}$$

where ρ_i is the density, z_0 is the position of Gibbs interface, and d is the alterable parameter concerning the interfacial thickness.[4]

When we obtain the fitting curves, we employ the "90-10" interfacial thickness criterion.[4] The interfacial thickness is defined as the distance between the positions where the densities of water or decane respectively reach 90% of their bulk densities. It is an ordinary practice to determine the interfacial thickness of the liquid-vapor or liquid-liquid interface.

1.4 Model validation

In our validation, firstly, by means of the fitting curves of the density profile we get the bulk densities of the water and decane phase, and compare them with the actual density under different temperature and pressure conditions. **Table S2** shows the comparison results. Our results are very close to the actual densities of the water and decane liquid under different conditions.

Further, we compare our simulated IFT of the decane-water interface with the results by other reseachers[4-11], including the simulated and experimental value, as shown in **Fig. S1**. Note that the simulated and experimental conditions of temperature, pressure and ion concentration in the referenced studies are a bit different from our simulation conditions. Moreover, the comparison of our results with the experimental results under high temperature or pressure is done, as shown in **Table S3**. As you can see, our simulated results of IFT are slightly smaller than the experimental results. We attribute this phenomenon to the difference in the temperature or pressure of the experiments. It is worth noting that the decane-water interfacial tension is sensitive to the inevitable impurities in the experiments, which we think play a key

role for the higher experimental results of IFT. Our simulation results are consistent with other results, indicating that our simulation model and method are reasonable and feasible for further researches.

Table S2. Simulated and actual densities of the water and decane bulk phase under different conditions.

	Conditions (K, atm)	**Actual density** ($g \cdot cm^{-3}$)	**Our results** ($g \cdot cm^{-3}$)
Water	300, 1	0.997	0.998
	320, 1	0.992	0.996
	340, 1	0.989	0.991
	300, 20	1.001	0.999
	300, 40	1.002	1.001
Decane	300, 1	0.725	0.723
	320, 1	0.710	0.712
	340, 1	0.694	0.697
	300, 20	0.726	0.723
	300, 40	0.728	0.729

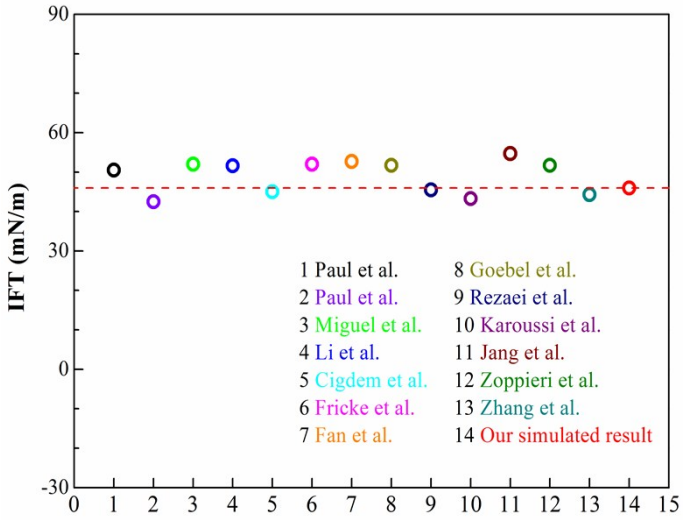

Figure S1. The IFT of the decane-water interface compared with the results of literatures (There is a slight difference for temperature, pressure and ion concentration).[4-11]

Table S3. The comparison of simulated IFTs with the experimental results in the literatures under high pressure or temperature conditions (For the sake of contrastive analysis, we only listed the experimental results of the conditions which close to our simulated conditions).

Authors et al.	year	IFT (mN/m)	T (K)	P (atm)
Susnar[12]	1994	51.64	294.65	3.8
		51.7	294.35	6.6
		51.79	294.35	35
Georgiadis[13]	2011	51.96	297.85	1.1
		47.78	323.35	1.8
		46.28	343.45	1.5
Cai[14]	1996	51.51	298.15	43.1
		49	323.15	38.7
Wiegand[15]	1994	51.1	295	1
		44.38	353	1
Zeppieri[16]	2001	51.98	298.15	1
		51.77	300.65	1
		50.13	318.15	1
		49.78	323.15	1
		49.21	333.15	1
Our simulated results	2017	44.34	300	40
		43.65	320	40
		41.72	340	40
		42.21	340	1
		41.91	340	20

2. Interfacial structure

2.1 Interfacial thickness

As previously stated, we can obtain the interfacial thickness of the decane-water interface systems with different ion concentrations (300 K, 1 atm), as shown in **Fig. S2**. With ion concentration increasing, the interfacial thickness decreases firstly, and then increases. At the ion concentration of 0.9 mol/L, the thickness reaches a minimum. This trend agrees with the results of IFT (see **Fig. 4(b)**). The greater IFT means the stronger immiscibility, thus the lower interfacial thickness.

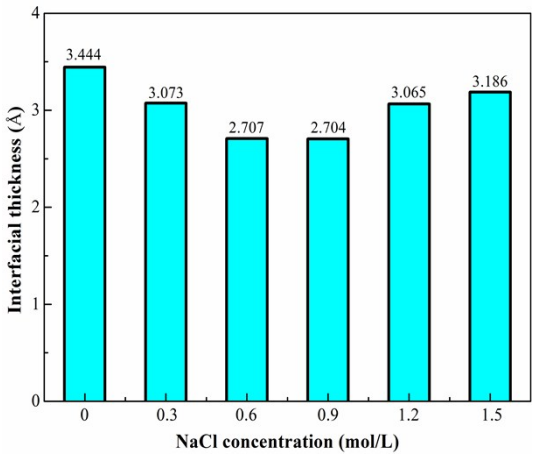

Figure S2. Interfacial thickness *vs.* ion concentration (300 K, 1 atm).

2.2 Adsorption of ions

According to the referenced studies[11], some kinds of ions can be adsorbed at or near the interface. **Fig. S3** shows the number density distribution of sodium and chloride ions near the interface. It can be seen that the chloride ions have the stronger affinity toward the interface than the sodium ions because of their weaker hydration, which will be discussed in section 3.2. The slight fluctuations of curves may be because the simulation time is not long enough or the ionic hydration hinders the motion of ions.

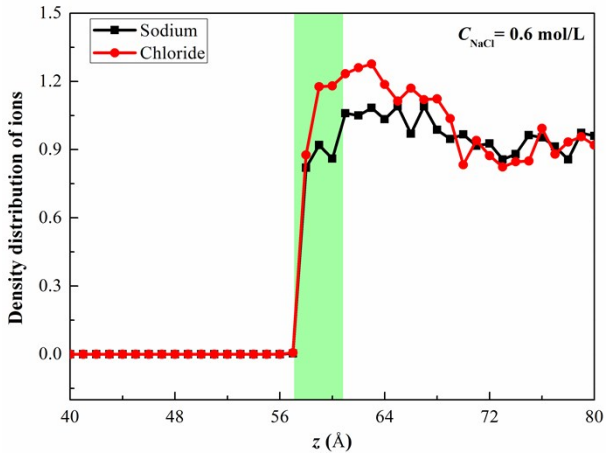

Figure S3. Distribution of ions along *z*-direction and at the decane-water interface. (The light green shadow represents the interfacial thickness)

3. Radial distribution function and ionic hydration

3.1 Radial distribution function

Fig. S4 shows the radial distribution function $g(r)$ of Na-Cl *versus* ion concentration. The fluctuations of curves may be because the simulation time is not long enough or the ionic hydration hinders the motion of ions. With ion concentration increasing, the distance r where the first peak occurs reduces, indicating that the sodium and chloride ions are gradually close to each other. It is noteworthy that the distance r where the first peak occurs at ion concentration of 1.5 mol/L is quite small and the peak value of $g_{Na\text{-}Cl}(r)$ is extremely higher than the other concentrations. The possible reason is that sodium and chloride ions are bound and exist in the water phase with the form of ion pair.

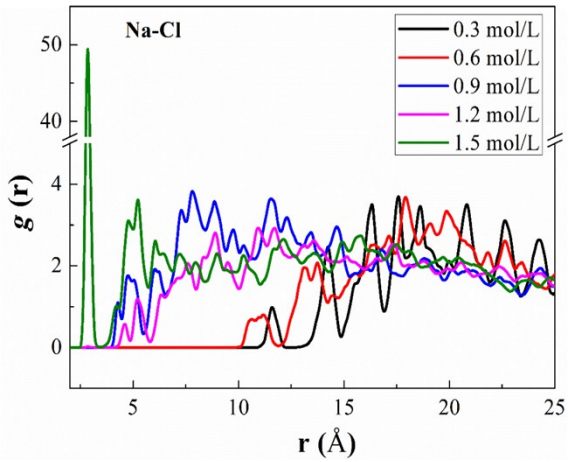

Figure S4. Radial distribution function of Na-Cl in the decane-water systems with different ion concentrations.

3.2 Hydration of ions

As we can see from **Fig. S5**, the decane molecules are likely to arrange themselves with carbon chain parallel to the interface and the dipole moment of water molecules also has the tendency to become parallel to the interface. The hydration of ions at or near the interface causes the aggregation of water molecules near ions, as shown in the right figure of **Fig. S5**. The number of hydrogen bond is greater for chloride ions than that for sodium ions because of their different hydrated structures. The oxygen atom of water in the first hydration layer of chloride ions is exposed to the water phase and has greater possibility to form hydrogen bond with other water molecules.

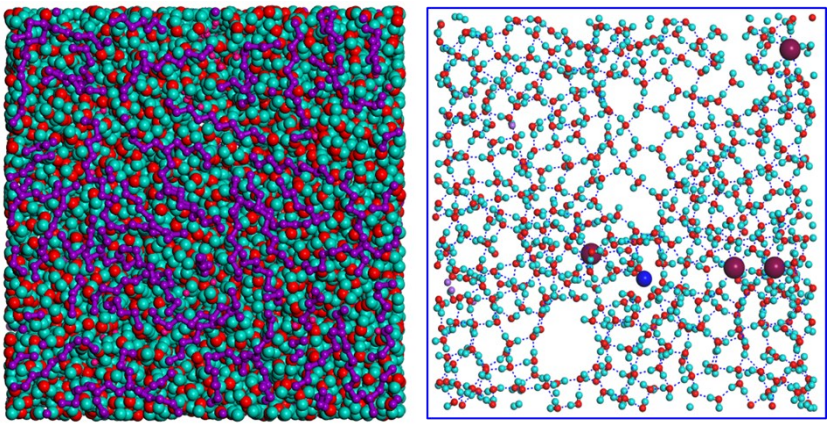

Figure S5. The conformation of decane (left), ions and water molecules (right) at or near the interface. (Purple: Decane molecules; Blue: Sodium ions; Brown: Chloride ions. The blue dashed line in the right figure represents the hydrogen bond)

The variations of ionic hydration at the interface under different ion concentrations are shown in **Fig. S6**. We can find that with the increase of ion concentration, more and more ions, particularly chloride ions, are adsorbed at the interface. From the enlarged view of the ionic hydrations, we can qualitatively conclude that the hydration of sodium ions is stronger than the hydration of chloride ions, which is quantitatively described in the section of **Hydration of ions** in the manuscript. At high ion concentrations (1.5 mol/L), the ions at the interface are close to one another owing to the more ions at the interface. A few oppositely charged ions can even bind together in the form of ion pair, as shown in the right map of **Fig. S6**. In terms of the significant effect of ion-pairs on IFT, we further calculate the number of ion-pairs at the interface (see **Table S3**). We find that the number of ion-pairs at the interface increases with ion concentration increasing. Particularly, a significant rise of the number of ion-pairs occurs at high ion concentrations (> 0.9 mol/L), which plays an important role in the decrease of IFT.

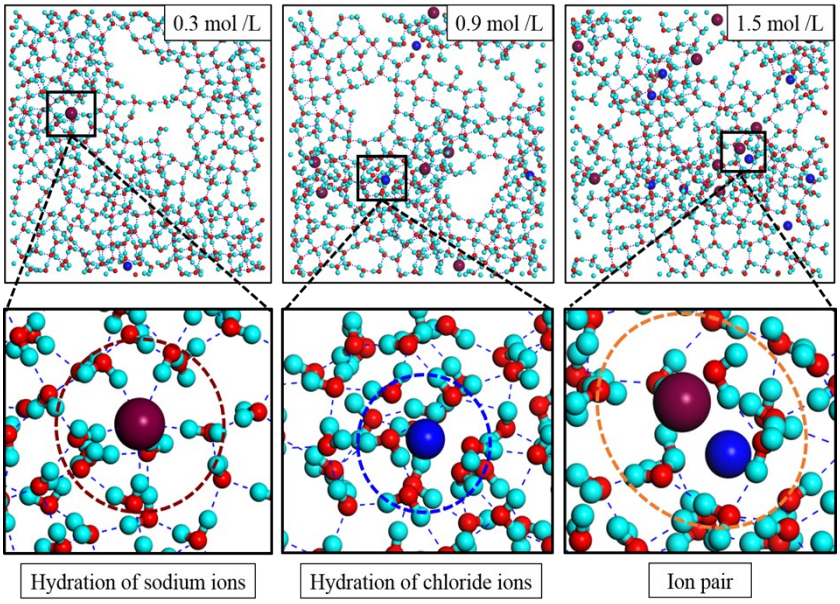

Figure S6. The ionic hydration at the interface under different ion concentrations.

Table S4. Number of ion-pair at the interface for the decane-water system with different ion concentrations (300K, 1 atm).

Ion concentration (mol/L)	0.3	0.6	0.9	1.2	1.5
Average number of ion-pair for every frame	0.028	0.431	0.643	1.960	2.926

For the sake of comparison, we run MD simulations with only one ion (sodium or chloride) at the interface. As we can see from Figure **S7**, the *z*-coordinate of ion fluctuates between the interface and the bulk phase, showing that the behavior of ion at the interface is a dynamic process including the adsorption, desorption and diffusion at the interface, as shown in illustration of Figure **S7** shown. For different ions with different hydration abilities, the residence time at the interface are different; namely, the sodium ion is strongly surrounded by water molecules and therefore stays at the interface for a short time while the chloride ion has the opposite trend. Since the residence time of ion at the interface is shorter than that in the bulk and the interaction between single ion and the interface is very weak, the time-averaged value (such as interfacial tension) in the simulations is almost the same as that of the decane-water interface without ions. Meanwhile, single ion at the interface cannot reflect the interactions between ions. Thus, the decane-water

interface without ions can serve as a reference to reveal the effects of interaction between ions on the interface tension and it is not necessarily to study the single ion at the interface.

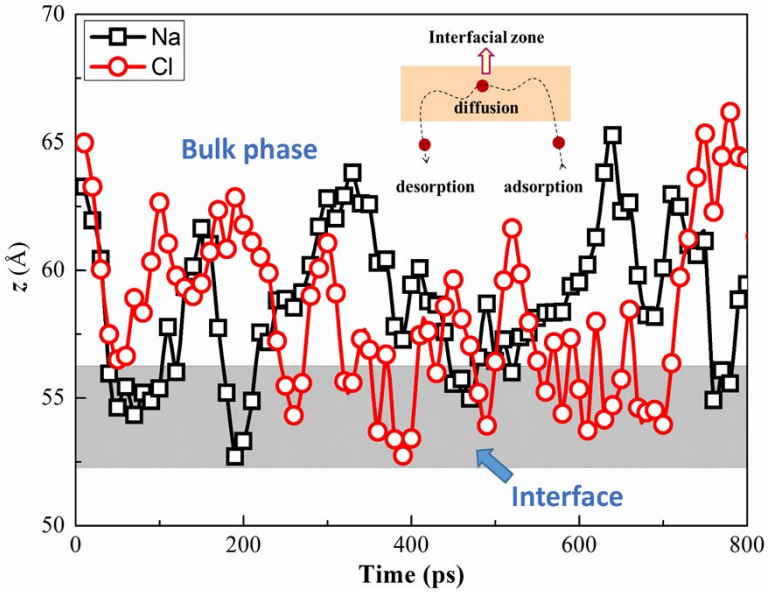

Figure S7. The *z*-coordinate distribution of single ion versus simulation time.

References

1. G. Kaminski, E. M. Duffy, T. Matsui and W. L. Jorgensen, *The Journal of Physical Chemistry*, 1994, **98**, 13077-13082.
2. S. W. I. Siu, K. Pluhackova and R. A. Böckmann, *Journal of Chemical Theory and Computation*, 2012, **8**, 1459-1470.
3. W. L. Jorgensen, J. Chandrasekhar, J. D. Madura, R. W. Impey and M. L. Klein, *The Journal of Chemical Physics*, 1983, **79**, 926-935.
4. S.-T. L. Seung Soon Jang, Prabal K. Maiti, Mario Blanco, and William A. Goddard III, *Journal of Physical Chemistry B*, 2004, **108**, 12130-12140.
5. P. D. Fletcher, L. D. Savory, F. Woods, A. Clarke and A. M. Howe, *Langmuir*, 2015, **31**, 3076-3085.
6. M. A. Fernandez-Rodriguez, J. Ramos, L. Isa, M. A. Rodriguez-Valverde, M. A. Cabrerizo-Vilchez and R. Hidalgo-Alvarez, *Langmuir*, 2015, **31**, 8818-8823.
7. C. O. Metin, J. R. Baran, Jr. and Q. P. Nguyen, *Journal of Nanoparticle Research*, 2012, **14**, 1246.
8. M. Fricke and K. Sundmacher, *Langmuir*, 2012, **28**, 6803-6815.
9. H. Fan, D. E. Resasco and A. Striolo, *Langmuir*, 2011, **27**, 5264-5274.
10. O. Karoussi and A. A. Hamouda, *Journal of Colloid and Iinterface Science*, 2008, **317**, 26-34.
11. C. Zhang and P. Carloni, *Journal of Physics: Condensed Matter*, 2012, **24**, 124109.
12. S. S. Susnar, H. A. Hamza and A. W. Neumann, *Colloids & Surfaces A Physicochemical & Engineering Aspects*, 1994, **89**, 169-180.
13. A. Georgiadis, G. Maitland, J. P. M. Trusler and A. Bismarck, *Journal of Chemical & Engineering Data*, 2011, **56**, 4900-4908.
14. B. Y. Cai, A. Jitao Yang and T. M. Guo, *Journal of Chemical & Engineering Data*, 1996, **41**, 493-496.
15. G. Wiegand and E. U. Franck, *Zeitschrift für Elektrochemie, Berichte der Bunsengesellschaft für physikalische Chemie*, 1994, **98**, 809-817.
16. S. Zeppieri, J. Rodríguez and A. López de Ramos, *Journal of Chemical & Engineering Data*, 2001, **46**, 1086-1088.